Neutron-Capture Cross Sections of the Stable Lead Isotopes*

B. J. Allen,† R. L. Macklin, R. R. Winters,‡ and C. Y. Fu
Oak Ridge National Laboratory, Oak Ridge, Tennessee 37830
(Received 21 May 1973)

Neutron-capture yields for several samples of separated lead isotopes were obtained at the Oak Ridge electron linear accelerator, in the neutron energy range above 2.5 keV. These were analyzed for resonance-capture areas and parameters. The data are included in a new evaluation of lead cross-section data.

[NUCLEAR REACTIONS ^{204,206,207,208}Pb(n,γ), $E_n > 2.5$ keV, measured $\sigma_{n,\gamma}$; deduced levels, E_γ, Γ, Γ_γ, averages, R.I., enriched targets, resolution ~0.2%.]

I. INTRODUCTION

The neutron-capture cross sections and resonance parameters of the isotopes of Pb in the keV neutron energy range are of considerable interest in studies of neutron physics, nuclear structure, astrophysics, and shielding applications.

Resonance-parameter systematics vary strongly near closed shells and the Pb isotopes present an opportunity to determine the influence of neutron shell closure at a closed proton shell. The observation of an s-wave doorway state[1] in ^{206}Pb and possibly ^{207}Pb which is based on a resonance at 500 keV in ^{208}Pb indicates the importance of detailed studies of these isotopes. We have therefore obtained parameters for resolved resonances from neutron capture in all four stable isotopes.

The lead isotopes also present a key to the chronology and temperature of stellar nucleosynthesis. Three distinct processes contribute to the observed abundances of the isotopes of Pb. One of these, the s process,[2] results from the capture of neutrons at keV energies during a low-intensity, sustained neutron exposure. A correlation between s-process abundances and Maxwellian-averaged capture cross sections is predicted, and the data presented here will permit a detailed analysis of the Pb-U chronology.[3]

The capture cross sections of the Pb isotopes together with γ-ray decay data permit accurate estimates of secondary γ-ray production cross sections in lead shields. Such information is of importance to integral experiments which utilize large lead detector shields and collimators. Results reported in this paper satisfy in part several requests in the RENDA and NCSAC request compilations.[4]

The high-resolution measurement of fast-capture cross sections with small (much less than one mole) samples of separated isotopes has become possible with the development of the Oak Ridge electron linear accelerator (ORELA).[5-7] Fast, efficient capture detectors such as the total energy detector (TED)[8] used in this experiment are essential together with an on-line computer system with high capacity semirandom access disc storage.[9] With a typical neutron energy resolution of 0.2% at 40 m, running times of the order of 24 h are sufficient for measurements on many separated isotopes. Consequently a comprehensive capture program is underway at ORELA to measure complete sets of isotopic cross sections for elements throughout the Periodic Table. The lead isotopes are the first of a series of reports on this work.

II. ORELA, DETECTORS AND COMPUTERS

Several papers have been published on the experimental procedure and associated equipment, and these have been referenced in the Introduction.[5-7,9] Consequently only an outline of the system is given in this section. A brief listing of conditions for runs used in the analysis to follow is given in Table I.

The capture facility at the 40-m flight station of ORELA is one of many experiments which operate on 11 flight paths. Typical running conditions for the capture measurements are: 140 MeV, 10-amp peak-pulse current, 8 kW for 5-ns pulses at 800 pulses per second. The flight path is equipped with a shadow bar (which reduces the sample scattered γ-ray flash to ~6 MeV as seen by the detectors), filters, and a series of copper collimators which define the beam to a 5.1-×2.5-cm cross section at 40 m. With a ^{10}B filter the beam is particularly clean, with a time-dependent background of less than 0.5% for neutron energies up to 35 keV and less than 1% at 105 and 1000 keV.

A major requirement of a neutron-capture de-

tector is that its efficiency be independent of the nature of the capture γ-ray spectra. Detectors often used are liquid scintillators (with almost 4π geometry) and Moxon-Rae detectors (with efficiency proportional to the total energy of excitation). A third type of detector called a total energy detector (TED) is used in this work. The application of a computed pulse-height weighting scheme results in an average response which is proportional only to the total energy (i.e., binding energy plus center-of-mass neutron energy). Two fluorocarbon liquid scintillators (Ne-226)[10] each 4 cm thick×10 cm diameter are mounted on 12.7-cm photomultipliers, and view the capture sample normal to the beam. The detectors have an efficiency per capture event of ~15% and a time resolution of better than 2 ns. At the 40-m station an energy resolution (in keV) of $E_n/600$ at 3 keV to $E_n/200$ at 2000 keV is obtained for 5-ns pulses.

One meter from the sample position a $\frac{1}{2}$-mm-thick ^{6}Li glass, viewed end on by two photomultiplier tubes, is used to monitor the incident neutron flux.[11] A plastic detector at the end of the beam tube provides a start pulse to a digital clock on detection of the γ flash, while an event from either TED or the ^{6}Li glass can stop the clock, the type event indicated by a tag word transmitted to the acquisition computer. The original clock designed by Nutt[12] has now been replaced with a TDC-100[10] time digitizer. This clock is normally operated in the single stop mode, with a 1024-ns delay, 1-ns time channels, and a 64-μs range. The pulse-height events from the TED's are digitized into 128 channels, which together with the 64 000 channels of time-of-flight data and various tags are sent to the on-line SEL810B computers for analysis and storage.

Calibration of the time-of-flight spectrum is achieved from transmission dips at 5906 keV in aluminum and higher energy resonances in sulphur at 30.4, 203, 274, 290, 375, and 587 keV. The pulse-height scale is frequently calibrated with the Compton edge of the 4.43-MeV ^{12}C γ ray from a Pu-Be source.

Two SEL810B computers (16 bits, 16 000 core) are available each with fast access disk storage. Each computer handles up to four separate experiments, accumulating data into a 512-word buffer before accessing the disk. Count rates of a few thousand events per second can be handled, although typical capture rates are only a few hundred events per second.

The 64 000 channels of time-of-flight data are crunched eight times before being loaded into four files each of 18 432 channels. Either the monitor or detector files are incremented with each event. In the latter case, a weight GWT (PH) is assigned to the detector event according to the observed pulse height (PH), and this weight is added to the appropriate time channel in the energy-weighted file. Similarly an unbiased and consistent estimate of the variance is stored. It is the GWT data which, after appropriate corrections, is proportional to the total energy emitted in a given time channel during the experiment (i.e., number of captures multiplied by excitation energy per capture). The standard deviation of the GWT is just the square root of the corresponding cumulative variance. In practice the GWT and variance files are each divided into four files corresponding to γ rays with energy above 285, 630, 1650, and 4080 keV. Thus it is possible to set a crude bias after an experiment by rejecting lower pulse-height groups. This was done for ^{207}Pb to determine the ground-state γ-ray yield from the 41-keV resonance.

A pulse-height spectrum is also accummulated in 128 channels (double precision) for all time-of-flight events from the TED's.

III. FLUX MEASUREMENT AND DETECTOR EFFICIENCY

The ^{6}Li(n, α) cross section has been reviewed recently by Uttley *et al.*[13] who specify an accuracy of 1% to 10 keV, increasing to 2% at 100 keV, 5% between 150 and 300 keV, and increasing to 10% at 500 keV. An accuracy of 15% is recommended between 700 and 1000 keV, and up to 1.7 MeV.

Earlier discrepencies in the energy of the p-wave resonance seem attributable to multiple-scattering effects in thick ^{6}Li glass scintillators. Thus the ^{6}Li(n,α) cross section is well known and a $\frac{1}{2}$-mm-thick ^{6}Li glass (NE-912) is now used at 39 m as the neutron flux monitor.[11] The energy of the p-wave resonance determined with this glass is ~240 keV, in excellent agreement with the Harwell work. The Uttley formalism is used to calculate the (n,α) cross section, with an additional resonance term at 2 MeV to fit the data above the 0.25-MeV p-wave resonance.

As the glass is upstream from the capture sample it is necessary to make corrections for flux perturbations as well as multiple scattering by the constituents of the glass (See Appendix I). The correction factors are best seen in Fig. 1, where the ratio of the efficiency per transmitted neutron (EFFTR) to the macroscopic cross section (XNA) is plotted. Without corrections this ratio would be unity. 90° scattering by glass constituents results in increased (n,α) yields as shown. EFFTR and the ^{6}Li(n,α) macroscopic cross section are shown separately in Fig. 2.

The neutron flux (ϕ) is determined from the observed ^{6}Li yield (Y_{Li}, i.e., $\phi(E) = Y_{\mathrm{Li}}(E)/\mathrm{EFFTR}$

(E), where E is the neutron kinetic energy in the laboratory frame of reference. For those measurements made before the installation of the glass, EFFINC (the efficiency for the incident or unperturbed beam) is used instead of EFFTR.

Assuming the thin sample approximation (i.e., σ_0^* APB ≤ 0.2, where APB is the atoms per barn of capture sample) and neglecting self-shielding and multiple-scattering corrections, the capture cross section (σ) is

$$\sigma(E) = N_c(E)/\epsilon\phi(E)\text{APB},$$

where $N_c(E)$ is the number of capture events at energy E and ϵ the detector efficiency for capture events. N_c is related to the weighted yield accumulated in the GWT spectrum by

$$N_c(E) = \text{GWT(PH)}/[\text{B.E.} + EA/(A+1)],$$

where the denominator is the total energy per capture, and GWT (PH) represents the product of the number of captures and the total energy per capture.

The capture efficiency of the TED's was determined by the application of the saturated resonance method to the 4.9-eV resonance of gold. As $\Gamma_\gamma \gg \Gamma_n$ for this resonance, the observed saturated capture yield for a 0.0030-atom-per-barn sample is proportional to the incident neutron flux because virtually all neutrons are captured. The weighted detector efficiency is thus $\epsilon = N_c(E)/\phi(E)$ where $\phi(E) = Y_{\text{Li}}(E)/\text{EFFTR}(E)$. A correction of 2.4% is calculated to account for the transmission on resonance and especially the backscattering from the gold foil.

A value of $\epsilon = 0.98 \pm 0.05$ was determined. This result is dependent on the discriminator settings of the associated glass electronics, and is periodically reevaluated. The neutron flux is also checked by the capture yield from a 0.05-cm gold foil sample used as a secondary standard. In addition, each run is monitored by a time-gated communal fission detector which can be used for normalization. Intercomparison of these methods suggests a reliability of flux measurement of $\pm 9\%$ [2 standard deviations (S.D.)] for the earliest runs (which include the ^{206}Pb and ^{208}Pb) and $\pm 5\%$ (2 S.D.) for the past year.

IV. DATA REDUCTION AND ANALYSIS

At the completion of a capture measurement the data are dumped onto magnetic tape for off-line reduction and analysis at the IBM-360 system. A dead-time correction is made to all data, based on combined count rate in the time-of-flight and monitor spectra. This correction utilizes the total number of beam bursts in a run. Time-independent background corrections are made for both the TED's (GWT) and glass (MON) and are based on beam-off count rates.

The time-dependent background is a more difficult correction to make. Part of this is related to the macroscopic potential scattering cross section. The ^{208}Pb spectrum exhibits few resonances and after these are removed a smooth yield curve is obtained which represents the background contribution from potential scattering. Structures at 6 and 27.5 keV (Fig. 3) are clearly observed which relate to sample scattered neutrons which are captured in the 5.906-keV resonance in the alumi-

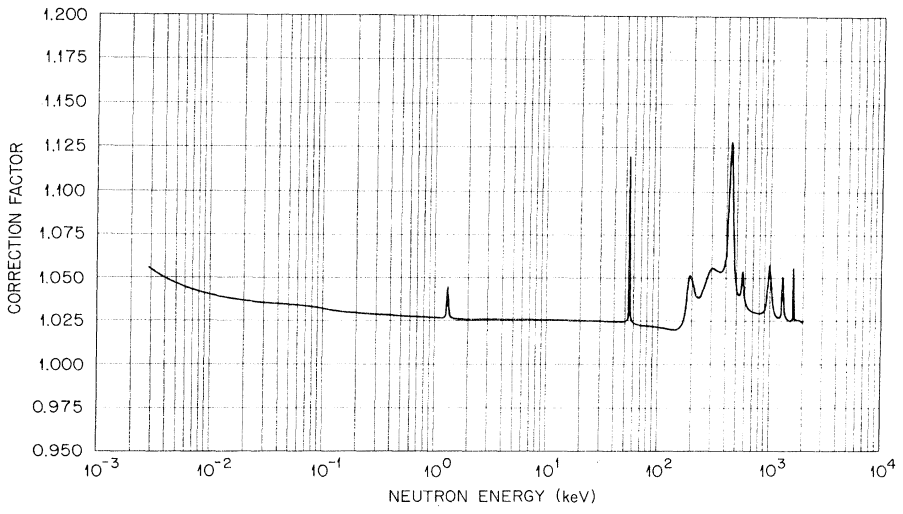

FIG. 1. Scattering, self-absorption, and resonance-structure effects for a 0.05-cm ^{6}Li glass scintillator; corrections calculated per transmitted neutron for use in determining neutron beam flux downstream from the scintillator.

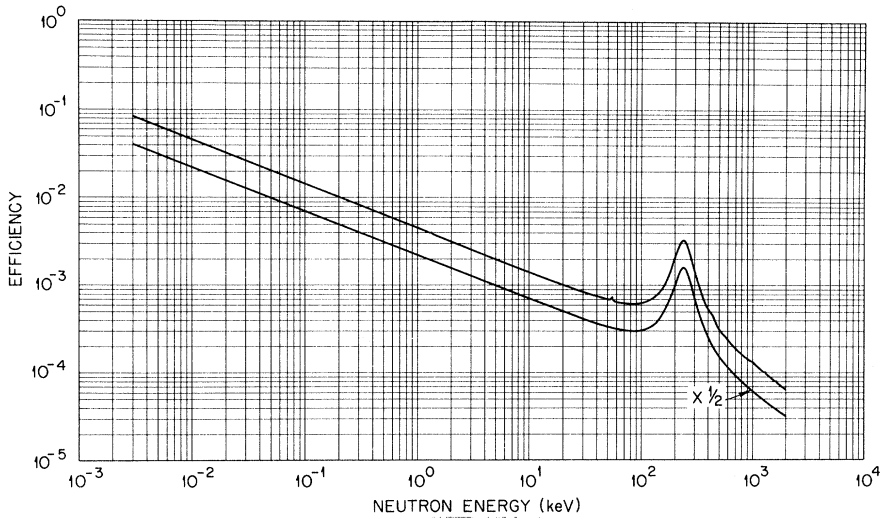

FIG. 2. Neutron efficiency for 0.05-cm ^{6}Li glass as a function of energy, per transmitted nwutron, using Uttley's ^{6}Li resonance parameters as modified (see text). The upper curve includes the corrections shown in Fig. 1, the lower is just proportional to the ^{6}Li(n,α) cross section used.

num beam tube and detector assembly and in the 27.07-keV resonance in the fluorine of the scintillator. After appropriate normalization of the macroscopic cross sections of the other lead isotopes relative to 208, the modified 208 yield is subtracted. For samples of light mass, the structure is shifted and spread to correspond to the analytic energy losses on elastic scattering. This method is validated by the elimination of the Al and F bumps from the isotopic yields. The remainder of the time-dependent background is present with no sample inserted in the beam and is measured in a separate run. The total background subtraction is typically 8 or 9%.

The time-of-flight spectra are converted to 12 linear energy groups from 2.5 keV to 2.5 Mev, by an interpolative procedure, and then normalized relative to the ^{6}Li(n,α) cross section. The final result is seen in Figs. 4–7 where the uncorrected cross sections for all four isotopes are compared as a function of energy. It is immediately apparent which resonances can be assigned as isotopic impurities. For many low-energy resonances the multiple-scattering events, appearing at higher calculated energies (shorter flight times) because of recoil-energy losses, are clearly resolved from primary-capture yield.

At higher energies in 204 and 206, where resonances become unresolved, the 208 correction is still assumed to be valid. Measurements with a 5-cm sulphur filter at 105 keV show that this assumption is justified to ~20%.

In addition to the background due to the nonresonant scattering from the sample, there also is associated with each resonance, a γ yield derived from neutrons scattered at the sample resonance and subsequently captured in the detector or housing. This scattered neutron sensitivity is typically a few parts in ten thousand.[14] It has been evaluated as a function of energy from the nonresonant ^{208}Pb scattering as indicated above. For narrow resonances it is negligible but can be appreciable for broad s-wave resonances.

In order to obtain resonance parameters the resolved resonances are analyzed by an automatic peak finding and Gaussian fitting computer code. The area, full width at half maximum, and Gaussian centroid are calculated, and these data are

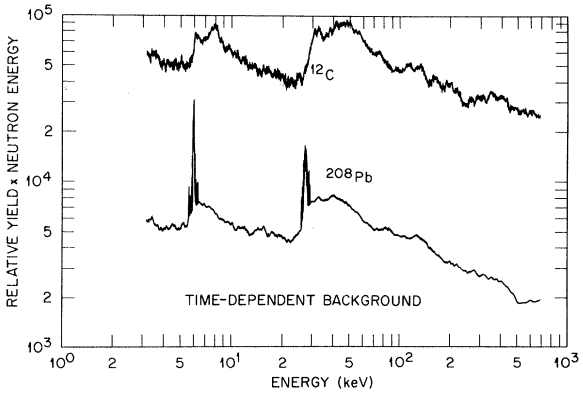

FIG. 3. Time-dependent backgrounds as seen with thick (6-mm) samples. Prominent features near 6, 27, and 35 keV are associated with capture in Al and F in and around the detectors after elastic scattering from the sample. The flux shape is closely proportional to $E^{-0.72}$ over the energy range 3–150 keV, implying an appreciable $E^{-0.5}$ or $1/v$ component in the background.

fed into a code which calculates energies, widths, and capture areas relative to the ^{6}Li(n,α) cross section. For many s-wave resonances the observed width is greater than the experimental resolution and it is therefore possible to obtain the neutron width directly. Again the thin sample approximation is used to obtain capture areas, using the equations already discussed. The radiative width Γ_γ can thus be obtained as

$$A_\gamma = 2\pi^2 \lambda\!\!\!^{-2}\, g\Gamma_n \Gamma_\gamma/\Gamma = \tfrac{1}{2}\pi\sigma_0\Gamma_\gamma ,$$

where $g=(2J+1)/2(2I+1)$ and σ_0 is the peak total cross section. In the case considered above $\Gamma \sim \Gamma_n \gg \Gamma_\gamma$ and $g\Gamma_\gamma = A_\gamma/2\pi^2\lambda\!\!\!^{-2}$.
With estimates of Γ_γ and Γ_n, self-protection and multiple-scattering corrections can be obtained using a resonance self-protection and average path-length code. If the observed resonance width is comparable to the experimental resolution, then $g\Gamma_\gamma\Gamma_n/\Gamma$ is obtained from the area analysis. In these cases, a somewhat more subjective judgement is necessary to obtain further results. If $g\Gamma_\gamma\Gamma_n/\Gamma \sim \langle g\Gamma_\gamma\rangle$, then it can be assumed that $\Gamma_n > \Gamma_\gamma$, but $\Gamma_n <$ resolution which allows the calculation of Γ_n for assumed values of $g\Gamma_\gamma$. Alternately if $g\Gamma_\gamma\Gamma_n/\Gamma \ll \langle g\Gamma_\gamma\rangle$ then $g\Gamma_n$ is obtained. Thus only approximate corrections can be made to the capture area under these conditions.

In the case of ^{207}Pb, where $\Gamma_\gamma \sim \Gamma_{\gamma\,\text{g.s.}}$, Porter-Thomas fluctuations are expected and it is not really possible to distinguish between Γ_n and Γ_γ unless $\Gamma >$ resolution.

Reduced neutron widths are calculated and strength functions and distributions of resonance parameters are obtained. The Maxwellian average capture cross section is determined as this is an important astrophysical quantity. The resonance integral is also given (see Table II).

For a number of low-energy resonances Monte Carlo calculations[15] have been made to fit the observed primary- and secondary-capture yields which are clearly resolved. These calculations serve as a check on the RSPAPL analytical corrections and permit estimates (not necessarily unique) of the resonance parameters to be made.

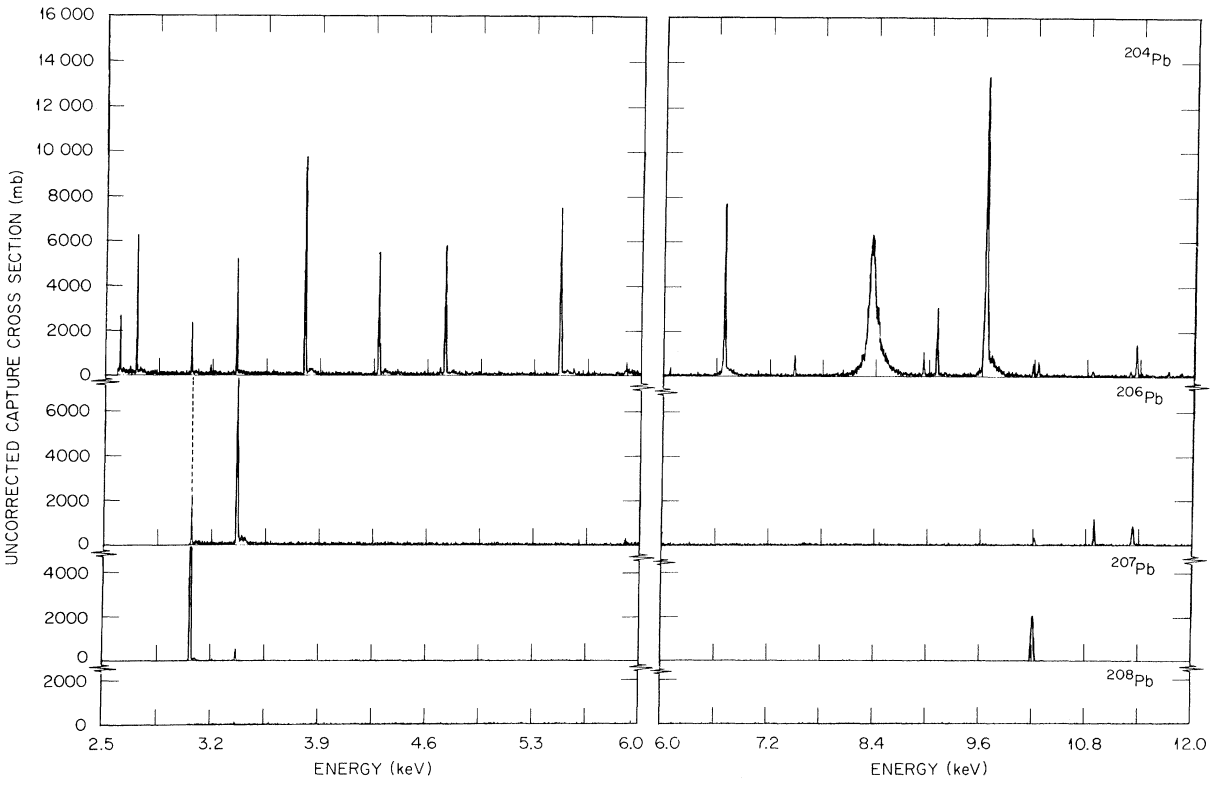

FIG. 4. Neutron capture yields of the lead isotope targets from 2.5—12 keV. Self-absorption in the peaks is corrected for in deriving resonance capture areas and parameters. Multiple scattering by the nonresonant cross section into the narrow peaks is seen as a small satellite centered at ~1% higher incident energy, corresponding to the 90° neutron elastic scattering energy loss for these nuclear masses.

V. DISTRIBUTION OF RESONANCE PARAMETERS

Because of fluctuations in parameters from resonance to resonance, it is the dependence on neutron energy and distribution of parameters relative to their mean values which are of interest. Thus Γ_γ should exhibit little spread, except in the case of ^{207}Pb where one decay channel dominates most resonances. Γ_n however is expected to fluctuate markedly though two cutoffs in the distribution will be apparent when for large Γ_n, Γ_n approaches the resolution limit, and for small $g\Gamma_n$ (derived from the area analysis) when capture areas are a few BeV. s-, p-, and possibly d-wave resonances will be observed and it is not possible from capture alone to determine the l value. However, if the neutron widths are considered to be of a predominant value then the average energy dependence of the l-reduced neutron widths allow a general l-wave assignment. Thus if the largest Γ_n show an $E^{1/2}$ dependence, then a general s-wave assignment is indicated. Similarly if the $E^{3/2}$ dependence is apparent for the smallest Γ_n group, a p-wave assignment is suggested. However, only if total cross-section data are available can individual l-wave assignments be made.

The data are further analyzed by plotting $X/\langle X\rangle$, where cutoffs and deviations from the expected χ^2 distributions suggest incorrect assignments.

It should be emphasized that the analysis does not, in general, produce a unique set of parameters, except in the resolved-width case when the total width Γ is greater than the experimental resolution.

The quality of the resonance data is best determined from a staircase plot of the cumulative number of resonances vs energy. If the staircase deviates substantially from linearity (Fig. 8), then many small resonances have been missed or pairs of resonances have not been resolved. Thus resonance analysis is best restricted to the linear region. This upper limit for the linear region is therefore noted in tables of resonance parameters.

With the exception of ^{207}Pb a large number of Γ_{γ_i} are expected to contribute to Γ_γ, such that $\Gamma_\gamma/\langle\Gamma_\gamma\rangle$ exhibits a χ^2 distribution with several degrees of freedom for resolved width resonances

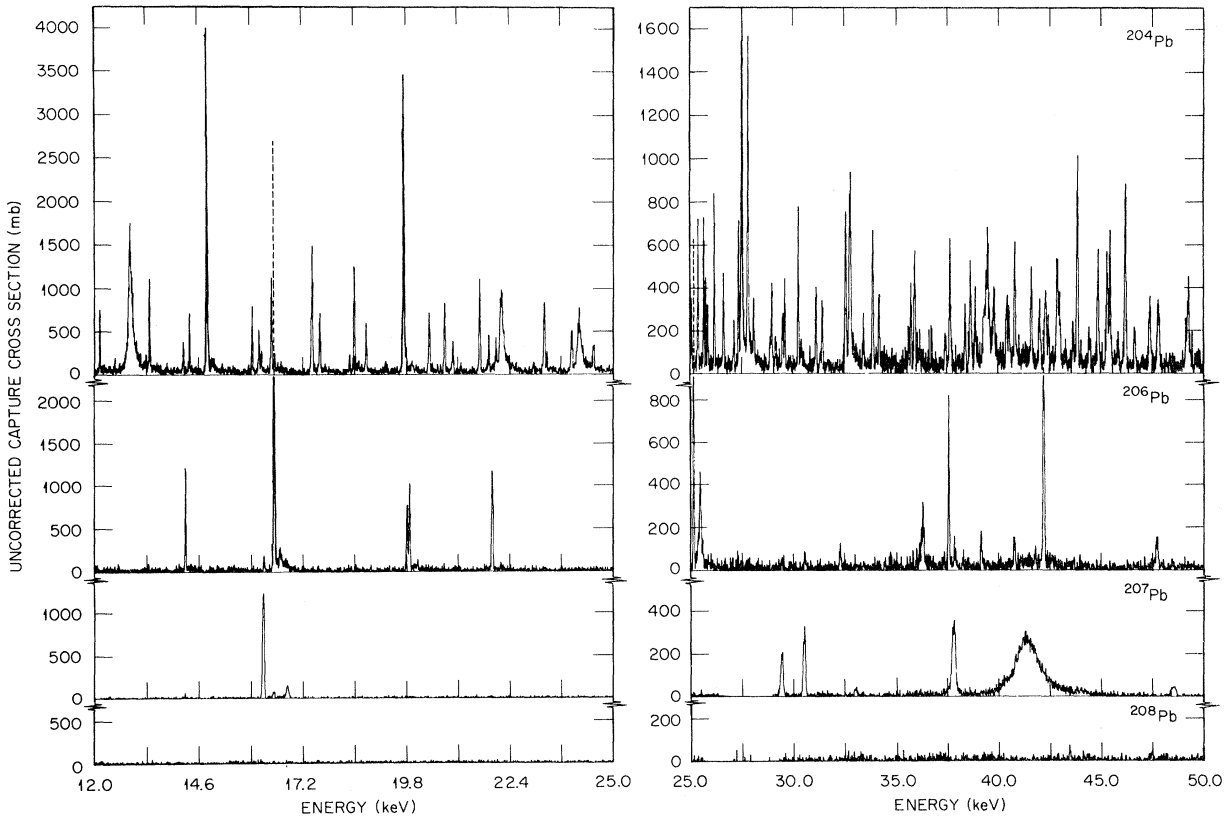

FIG. 5. Yields for 12—50 keV. The dramatic effect on neutron shell closure (N=128) on level density almost obliterates the customary odd-neutron-number enhancement. A shape analysis of the 41-keV peak in ^{207}Pb(n,γ) and ^{207}Pb(n,γ_0) has been reported separately (Ref. 17).

TABLE I. Sample and accelerator data for the runs used in the analysis. APB is atoms of isotope per barn. DT corr is dead-time correction at ~50 μs after the γ flash.

A	A (%)	APB	Pulse width (ns)	DT corr	Burst rate (sec^{-1})	Bursts ($\times 10^6$)	Power (kW)
208	99.75	0.0231	8	1.08	500	82.2	5
207	92.4	0.0013	40	1.07	500	283.6	20
		0.0282	5	1.08	800	24.1	9
206	88.38	0.0136	5	1.05	500	48.4	5
204	71.41	0.0067	5	1.24	800	43.5	7.5

TABLE II. Average parameters for the resonances seen in neutron capture by the stable lead isotopes.

	204	206	207	208
Linear range (keV)	60	240	125	1050
$\langle\Gamma_\gamma\rangle$ (eV)	0.5±0.05	1.6±0.2	0.6±0.15	2.2±0.7
S_γ [a]	$>1.9\times10^{-4}$	$>1.4\times10^{-4}$	$>0.9\times10^{-4}$	$>0.3\times10^{-4}$
S_0 (adopted)	2.2×10^{-4}	0.8×10^{-4}	0.9×10^{-4}	0.35×10^{-4}
S_1			$<1.8\times10^{-4}$	
No.	149	56	26	37
No. analyzed	22	20	18	9
D (keV)	0.4±0.04	4.3±0.5	4.8±0.6	28±6
$\nu(g\Gamma_\gamma/\langle g\Gamma_\gamma\rangle)$	~5	~2	~1	
$\frac{\langle\sigma v\rangle}{v_T}$ (mb) [b]	74±5	14±1	11.3±0.7	0.75±0.09
RI (mb)	726±22 [c]	86±6	381±23	2.8±0.3

(with $\Gamma >$ res.). Consequently those values of $g\Gamma_n\Gamma_\gamma/\Gamma$ obtained for unresolved resonances which lie within the obtained Γ_γ distribution are taken to be a measure of Γ_γ. For these resonances Γ_n is presumed to be $>\Gamma_\gamma$ but less than the experimental resolution. Values of $g\Gamma_n\Gamma_\gamma/\Gamma$ which lie below the Γ_γ distribution are assumed to be a measure of $g\Gamma_n$. These values are plotted as the reduced widths $g\Gamma_n^l$ to determine the most probable l assignment. As g is generally unknown the variation in g complicates the $g\Gamma_\gamma/\langle g\Gamma_\gamma\rangle$ analysis. If the energy dependence of the resolved widths supports an s-wave assignment $g=1$ for the even isotopes and $\frac{1}{4}$, $\frac{3}{4}$ for ^{207}Pb. If p-wave assignments are also probable then the possible

[a] $S_\gamma = \sum_{E_1}^{E_2}\Gamma_{\gamma\lambda}/(E_2-E_1)$.

[b] $v_T=(2kT/m)^{1/2}$ for $kT=30$ keV and m the reduced mass.

[c] The resonance at 1.69 keV was estimated to contribute 28 mb.

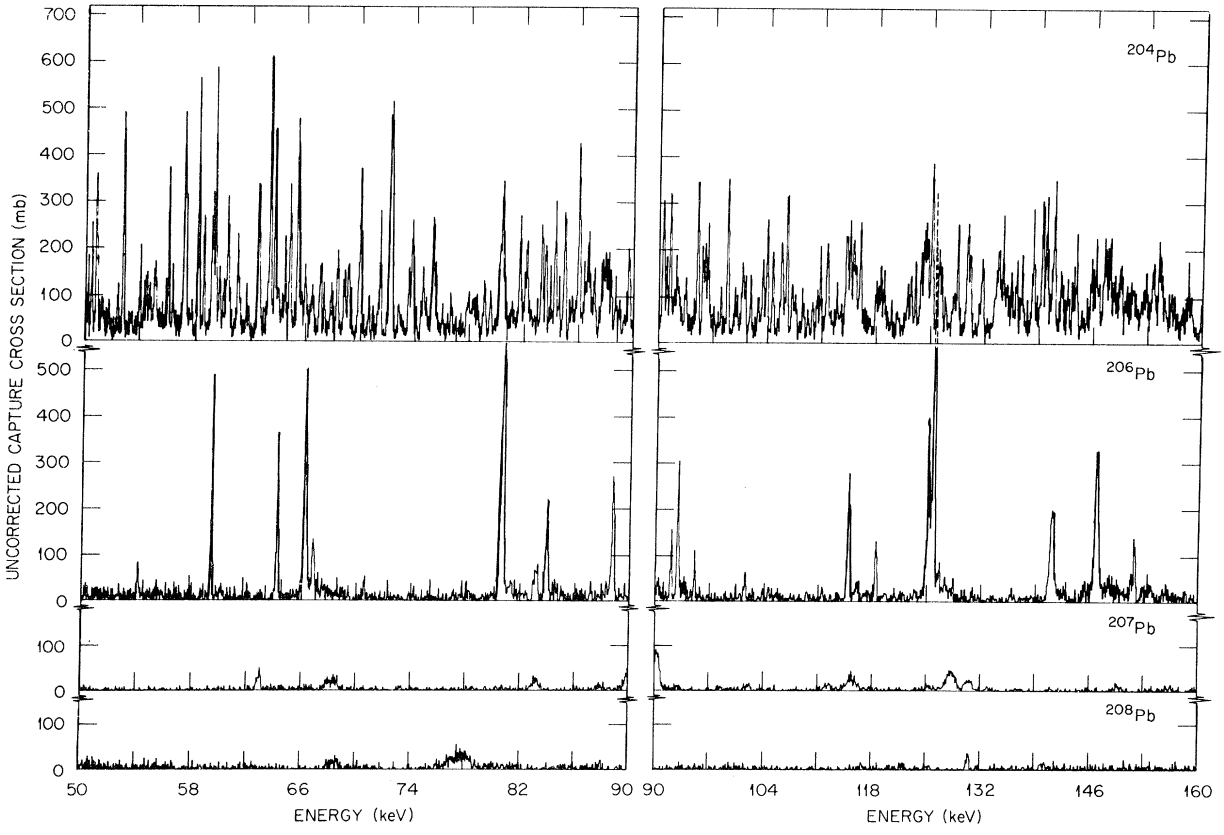

FIG. 6. Neutron capture yields from 50 to 160 keV. The lowest resonances in ^{208}Pb + n appear at 66.8 and 77.7 keV with another near 131 keV.

TABLE III. Individual resonance parameters significant in neutron capture by natural lead and comparisons with earlier work and a recent evaluation.

	This work				Good					BNL-325					Adopted [a]		
Isotope	E_n (keV)	Γ (eV)	$g\Gamma_\gamma$ [b] (eV)	A_γ [b] (BeV)	E_n (keV)	Γ (eV)	A_T [c] (BeV)	Γ_n (eV)	$2g\Gamma_n$ (eV)	Γ_γ (eV)	$g\Gamma_\gamma$ (eV)	Γ (eV)	J	l	E_n (keV)	Γ (eV)	Γ_γ (eV)
204					1.690	5	79	3.9		≲2		<5.9	½	0	1.685	5	
204	2.596	<5	0.03	0.59	2.485	8	100	5.8		≲2		<7.8	½	0	2.485	5	0.02
207	3.071	<7		21	3.070	2	25		~0.3	≲5					3.070	2	0.93
206	3.365	<6.6		16	3.364	5	74		~0.9	<2				1	3.360	5	0.57
204	8.348	56±8	1.9	10.3	8.374	67	320	50		≲10		<60	½	0	8.350	56	1.5
204	9.635	<19	1.0	4.2	9.680	30	61	15		≲10		<25	½	0	9.635	19	0.87
207	10.21	<24		12	10.21	21	61								10.21	21	
207	12.40	17±5	0.004	0.34	12.39	24	82					11–25		1	12.39	17	
204	12.88	91±9	0.7	2.6	12.92	77	240	45		≲10		<55	½	0	12.90	55	0.67
206	14.25	<29		5.2	14.24	24	68								14.24	24	
207	16.21	<38		16.2	16.20	44	65							1	16.20	38	
206	16.47	<34		39	16.47				8	<5	0.8	<20		1	16.47	20	
207	16.80	60±7	0.06	3.2	16.80	61	730		68	<5	0.3	36–91		1	16.80	60	0.15
206	19.80	<41		5.9	19.79	49	98								19.79	41	
206	19.86	<42		6.1											19.86		
206	21.94	<45		9.4	21.93	33	32								21.93	33	
206	25.17	<53		15											25.17		
206	25.49	102±15	0.34	13	25.47	100	1060		120	<10	0.77	34–49		1	25.47	59	
207	29.46	<72		6.6	29.44	82	320		160		0.35	23–65			29.44	65	
207	30.54	<75		8.7	30.43	30	60								30.48	30	
206	37.57	<80		8.6	36.27	120	400								36.90	58	
207	37.82	98±9	0.75	18	37.78	160	650					22–70			37.80	70	
207	41.32	1268±150	3.7	85	41.64	1770	16 000			5.5		1244	1	0	41.60	1250	5.0
206	42.20	<90		17											42.20		
206	47.70	<103		2	47.61	220	1200								47.60	73	
206	59.39	<130		11											59.39	130	
206	64.16	<140		7.5											64.16	140	
206	66.19	116±10	1.27	19	66.22	200	600					250	½	0	66.20	116	
206	70.50	<155		1.3	71.31	360	2800								71.00	155	
208	77.70	2252±340	1.2	34	78.22	1370	26 400					1000	½	1	78.00	1000	1.26
206	80.63	<180		26											80.63		
206	83.90	134±25		8.9	86.71	620	1750		420					1	85.00	134	
206	88.77	<200		11											88.77	200	
207	90.40	674±100	2.0	20	90.29	850	3700								90.35	674	
206	92.04	151±22		5											92.04	151	

TABLE III (*Continued*)

Isotope	This work E_n (keV)	This work Γ (eV)	This work $g\Gamma_\gamma$ [b] (eV)	This work A_γ [b] (BeV)	Good E_n (keV)	Good Γ (eV)	Good A_T [c] (BeV)	Good Γ_n (eV)	Good $2g\Gamma_n$ (eV)	Good Γ_γ (eV)	BNL-325 $g\Gamma_\gamma$ (eV)	BNL-325 Γ (eV)	J	l	Adopted [a] E_n (keV)	Adopted [a] Γ (eV)	Adopted [a] Γ_γ (eV)
206	92.90	149 ± 18		14											92.90	149	
206	114.9	264 ± 50	2.7	24	115.5	800	1500								115.2	264	
206	118.4	<270		7	117.4	840	5600								117.9	270	
206	125.1	250 ± 50	3.7	29	124.8	620	2400								125.0	250	
206	125.7	<166		57	128.0	500	1600		920					1	127.0	166	
206	141.1	409 ± 50	3.4	23	140.2	530	910								140.6	409	
206	146.8	400 ± 50	5.7	38											146.8	400	
206	151.7	370 ± 65		7.3	150.2	1400	6800		1800					1	151.0	370	
206	170.0	<300		6.4	169.0	1700	2100								169.5	300	
207	181.9	306 ± 40	12.5	64	180.5	1000	1400								181.0	306	
206	199.2	383 ± 50		26	198.5	1200	1300		520					1	198.5	383	

[a] For use with triangular resonance shape assumption except 41.32 keV, ENDF/B-III Files (Ref. 22).
[b] Errors are generally dominated by normalization uncertainties, thought not to exceed 10% (S.D.).
[c] All areas computed for natural lead, using isotopic abundances 0.0124, 0.236, 0.226, and 0.523 for the isotopes 204, 206, 207, and 208, respectively.

spread in g increases and results in a lower value for the degrees of freedom of the observed distribution. Various aspects of the data are now considered for each isotope:

^{208}Pb. A number of low-energy resonances observed in the capture yield are assigned to minor isotopic impurities while structure observed at 6 and 27.5 keV is the result of the detector sensitivity to scattered neutrons. Resonance parameters are given in Table III. An effort was made to extend the data above 1 MeV for comparison with earlier Van de Graff results.[16,17] However, the γ-ray yield of the TED system may not have been entirely reliable in this energy range because of electronic recovery from γ flash effects. Further uncertainty results from a lack of knowledge of the shape of the background which increases above 1050 keV because of inelastic scattering in the aluminum housing. However, agreement in energies and neutron widths is satisfactory. Our capture data show an unusual group of eight resonances in the energy range 700–800 keV which contain most of the radiative strength below 1 MeV (total capture area 220 b eV). Fowler[16,17] has determined the spins and parities of some of these resonances to be $d_{3/2}$, $d_{5/2}$, and $p_{3/2}$. Others are very weak in the total cross section or have not been resolved. While this envelope of radiative strength is suggestive of a doorway interaction the presence of at least three different types of resonances negates such a simple explanation. Further, there is no obvious correlation between $g\Gamma_\gamma$ and Γ_n, or J. The γ-ray decay from these resonances is limited to only a few final states (i.e., three $d_{5/2}$ at 1.57, four $s_{1/2}$ at 2.03, and three $d_{3/2}$ at 2.54 MeV) and it might be expected that the valence model should be applicable here for strong single-particle $E1$ and $M1$ transitions. However, this is not observed as Γ_γ for the $p_{3/2}$ resonance ($E1$ transitions to $d_{5/2}$, $s_{1/2}$, $d_{3/2}$) remains comparable to that for the $d_{3/2}$ ($M1$ transitions) although its strength is expected to be strongly dependent on the $E1/M1$ ratio (> 5).

The strong s-wave resonance at 500 keV is not observed in the capture data. Because $\Gamma_n \sim 60$ keV for this resonance, the capture area ($=g\Gamma_\gamma$) is spread out over too large an energy range and lost in the statistics. ^{208}Pb represents a classical example of the ability of capture measurements to detect higher l-wave resonances which are not observed in the total cross section, while a strong s-wave resonance is effectively hidden.

^{207}Pb. Two measurements were made with different sample thicknesses and pulse widths (see Table I). Energies and widths were obtained from the high-resolution run and capture areas (with smaller self-shielding and multiple-scattering

corrections) were obtained from the thin sample run. Resonance parameters are given in Table III where older (n,γ) and total cross-section data are also given for comparison.

Capture cross-section measurements normally determine total radiative widths when $\Gamma_\gamma \ll \Gamma_n$. However, in this particular case it was also possible to extract ground-state partial radiative widths by setting a bias at 4080 keV on the pulse-height spectrum, such that only the ground-state (g.s.) yield is observed. The results so obtained can be normalized to the 41.2-keV resonance where $\Gamma_\gamma = \Gamma_{\gamma_0}$. The ground-state branching ratio $(B_0 = \Gamma_{\gamma_0}/\Gamma_\gamma)$ can be used to assign resonance spins in some cases. Only 1^+ or 1^- resonances can reach the 0^+ ground state by $M1$ or $E1$ transitions, with very little strength to the 3^- low-lying excited states. Transitions from $0^\pm$ resonances to the g.s. are forbidden while those from resonances with $J^\pi \geq 2^\pm$ would be very weak. Consequently when $B_0 \sim 1$, a $1^\pm$ assignment is indicated. Such assignments confirm the observation of Bowman *et al.*[18] of the near exhaustion of the $M1$ giant resonance below 1 MeV. The total γ width of p-wave resonances found up to $E_n = 640$ keV was 36–53 eV. This was based on 12 resonances identified as 1^+, 14 assigned 2^+, and half of the 16 with unassigned parity.[19]

Estimates of s- and p-wave strength functions are also obtained (see Table II).

The analysis of this isotope above the inelastic neutron threshold at 570 keV is complicated as

$$\Gamma_{n_{\text{obs}}} = \Gamma_n + \Gamma_{n\,\text{inel}}$$

and

$$\Gamma_{\gamma_{\text{obs}}} = \Gamma_\gamma + \Gamma_{n\,\text{inel}} \frac{570\ \text{keV}}{[BE + (A/A+1)E_n]} \ .$$

Consequently parameter distributions are only considered up to 570 keV. Figure 8 shows clearly the onset of $(n,n'\gamma)$ where the level density is observed to suddenly increase. A similar effect is observed in the γ energy yield which increases rapidly above the threshold. The plot number of resonances vs energy shows that few resonances are missed up to 125 keV, but from 180–570 keV there is an unusual dearth of resonances, but not of radiative strength. A careful examination of

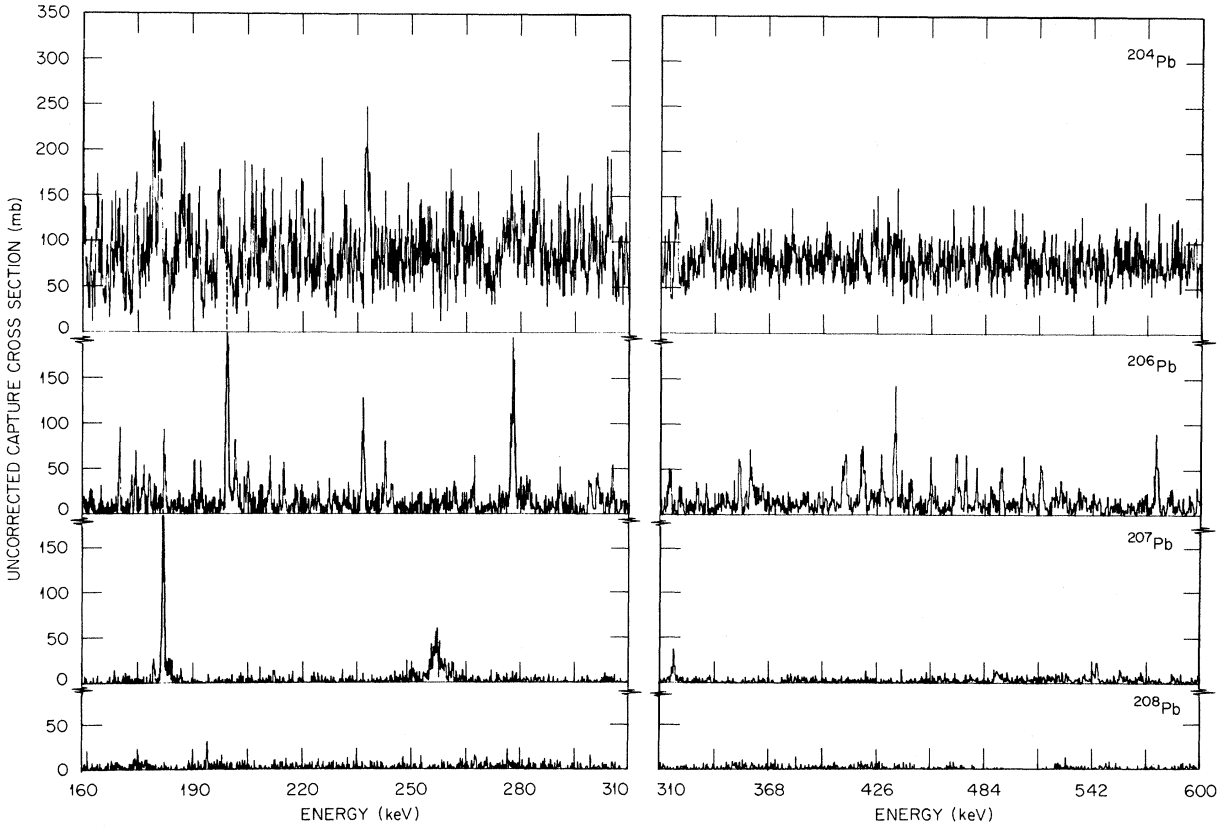

FIG. 7. Neutron capture yields from 160—600 keV. The structure in ^{204}Pb + n is clearly too dense for single resonance analysis. Some of the structure in ^{206}Pb + n has been analyzed (Ref. 18) for its interest to s-wave doorway-state observations.

the experimental data shows that this effect is real, although the onset of a high-level density above 570 keV indicates that small resonances have been missed and are now observed because of their inelastic scattering component. Only resonances with $J^\pi = 1^+, 2^\pm, 3^-$ should lead to prominent scattering to the 570-keV first excited state in the first 100 keV or so above its threshold because of the outgoing neutron's angular momentum barrier for $l_n \geq 2$.

Analysis of the shape of the 41.17-keV resonance, important to an evaluation of nonresonant capture, has been reported separately.[19] The distribution of radiative widths (Fig. 9) is quite broad as expected from the dominance of ground-state transitions. A χ^2 fit with one degree of freedom fits the distribution well [$\nu(\Gamma_\gamma/\langle\Gamma_\gamma\rangle) \cong 1$ in Table II].

^{206}Pb. The stronger analyzed resonances below 200 keV are included in Table III. The question of an $s_{1/2}$ doorway-state enhancement in the higher (incompletely resolved) energy region is discussed separately.[20]

The over-all distribution of the radiative widths for resolved resonances follows a χ^2 distribution with approximately two degrees of freedom (see Table II), indicating that in general only two decay modes dominate—presumably to the $\frac{1}{2}^-$ g.s. and $\frac{3}{2}^-$ second excited state. Area analysis yields $g\Gamma_\gamma\Gamma_n/\Gamma$ which is largely energy-independent, suggesting that $\Gamma_n \gg \Gamma_\gamma$. Thus the distribution of $g\Gamma_\gamma$ for all resonances has $\nu \sim 1.5$, in close agreement with that obtained for the resolved width resonances only.

^{204}Pb. Because of the high level density, resonances appear to be missed in ^{204}Pb above 60 keV, where the $\sum N(E_n)$ staircase plot deviates substantially from linearity. The spacing distribution shows a decreasing component of small values as the upper energy cutoff is reduced. The distribution observed for the broader resonances below 60 keV is found to fit quite well that expected for a Wigner distribution of a population of a single spin state. This result is in keeping with the expected s-wave character of the larger resonances.

Comparison of resonance parameters. In general there is little published data of comparable resolution on the Pb isotopes available for comparison. High-resolution measurements of ^{208}Pb(γ, n) give ground-state radiative widths which can be compared with our high bias ^{207}Pb(n, γ) results.[19] ORELA total cross-section measurements for natural Pb are also available. As it is the resonance parameters of natural Pb which are of interest in shielding applications, isotopic capture results normalized to isotopic abundances are compared with total cross-section results in Table III. An evaluation of the data is also given (see Sec. VII).

VI. AVERAGE CAPTURE CROSS SECTIONS

Because of the high resolution of the ORELA capture cross-section measurements comparison with earlier results is not readily achieved. By averaging the data over broad energy intervals[21] results are obtained which are effectively independent of energy resolution. It is also possible to check the types of analysis used in this work in the resolved resonance region.

The resonance analysis discussed in the preceding section is based solely on peak fits on slowly varying backgrounds. However, to obtain cross sections in the unresolved resonance region it is necessary to make accurate estimates of the

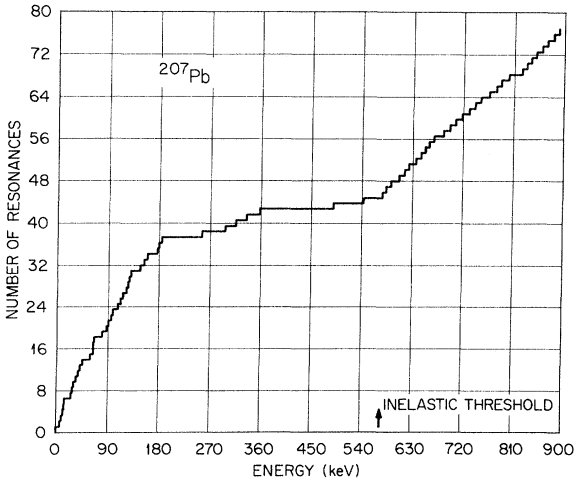

FIG. 8. Cumulative distribution of the analyzed resonances for ^{207}Pb + n.

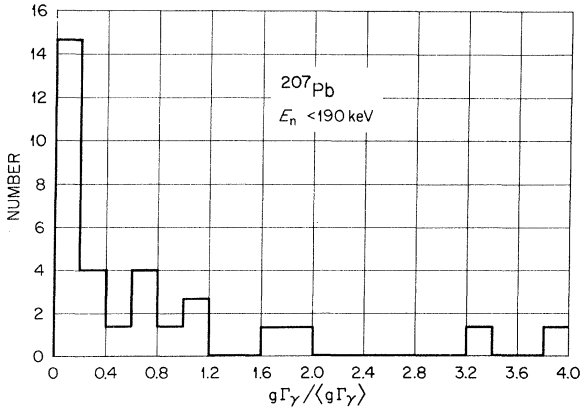

FIG. 9. Distribution of radiative widths for ^{207}Pb + n below 190 keV where Fig. 8 indicates that few resonances were missed. The dominance of the ground-state transition from ^{208}Pb* leads to an unusually wide range (see Sec. V).

time-dependent backgrounds as a function of neutron energy (see Sec. IV). Typically as resonances are missed the cross sections deduced from the resolved resonance analysis will decrease. On the other hand the background subtraction must be accurate (and retain negative as well as positive residuals) in order to obtain near-zero cross sections between resonances.

In order to calculate resonance self-shielding and multiple-scattering correction for the average cross-section analysis in 204 and 206, the parameters $\langle\Gamma_\gamma\rangle$, D, S_0, and S_1 are required for input for the code. The resolved resonance analysis provides estimates of these parameters except for S_1 which is obtained from strength function systematics.

The average cross sections of the lead isotopes are given elsewhere.[21] Two specialized average cross sections are included in Table II. The dilute resonance integral $\int \sigma dE/E$ above the cadmium cutoff is useful in strongly moderated neutron

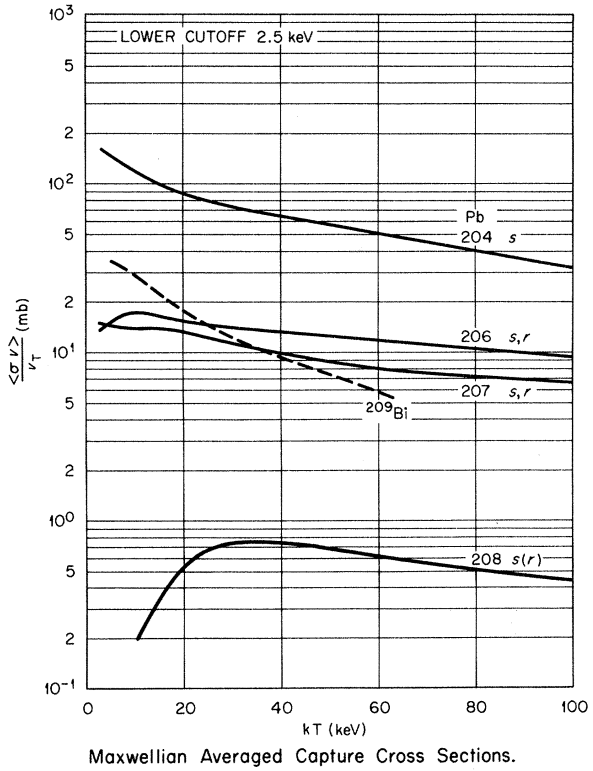

FIG. 10. Neutron capture cross sections for the stable lead isotopes averaged over Maxwellian flux distributions typical of the temperatures inside stars. Natural ^{204}Pb is calculated to have been produced only by slow neutron capture in stars whereas the heavier lead isotope abundances have been augmented by α (and β) decay of transbismuth isotopes and by β decay of neutron-rich supernova ejecta.

populations, typically thermal reactors where the flux shape (above thermal energies) approximates a $1/E$ dependence. For astrophysical nucleosynthesis applications the cross sections are averaged over the "thermal" neutron-flux distributions typical of the interior zones of a star. A Maxwellian with $kT = 30$ keV is convenient as the cross sections for many isotopes scale similarly with kT. For the stable lead isotopes the sparse level population near $A = 208$ leads to an appreciable departure from the usual case as shown in Fig. 10. As the nucleosynthetic s-process is recycled by α decay just above $A = 209$ (bismuth) this temperature dependence has not led to a unique stellar thermometer as originally hoped.

VII. EVALUATION

Table III displays some results analyzed from a cross-section evaluator's viewpoint. The ENDF/B-III cross-section file for material 1136 (natural lead) has been evaluated and maintained at Oak Ridge National Laboratory.[21] The present measurement of capture cross sections should enhance the capture cross-section file substantially in view of the sparseness of the previously available data. At present it is not practical to represent all the capture resonances (numbering more than 500) explicitly in the cross-section file. Table III lists only those capture resonances which could be correlated with the observed resonances in the total cross section, and those having areas greater than 5 BeV in terms of natural lead. All areas in Table III are given in terms of natural lead using isotopic abundances of 0.0124, 0.236, 0.226, and 0.523 for the isotopes 204, 206, 207, and 208, respectively. It is desirable to represent these capture resonances in the same energies and widths as the total resonances such that, upon subtracting the former from the latter, elastic scattering resonances will be reasonably represented. The remainder of the capture resonances, together with the $1/v$ component, were averaged to form a smooth background.[21] Total widths (Γ) and resonance areas (A_T) in the total cross section were calculated from the resonance parameters ($2g\Gamma_n$ or equivalent) compiled in BNL-325[22] and are compared in Table III with those derived from an ORELA measurement by Good[21] (the parameters shown there were derived from preliminary transmission data by Fu and Perey. Good has since obtained further data to be published separately). The adopted E, Γ, and A_T are averages of the available data with the following exceptions. Below approximately 50 keV, the areas of Good's measurements are on the average 50% lower than those taken from BNL-325. We

adopted the total areas from BNL-325 where available and increased by 50% the areas of the other resonances in Good's data. Most of the total widths from the capture measurement are given as upper limits. Because the capture measurement has the better energy resolution, these limits should not be violated. Thus if the total widths from BNL-325 and from Good's measurement are greater than these upper limits, these limits were adopted as the total widths. For the capture resonances which have areas greater than 5 BeV but which could not be correlated with the total, we used $A_T = A_\gamma$ for the sole purpose of explicitly representing these large capture resonances in the ENDF/B file. For some of the resonances for which A_T and Γ appear reasonably certain, one can extract Γ_γ values, which are listed in the last column of Table III.

APPENDIX I.

While a thin (< 1-mm) ^{6}Li glass scintillator inserted in a neutron beam produces only a minor flux perturbation, the departure from transparency is not quite small enough to ignore. When the light pulses from the glass are used to measure the flux as well [via the ^{6}Li$(n,\alpha T)$ cross section], processes wherein a neutron is first scattered in the glass before capture by ^{6}Li produce even larger effects through enhancement of the efficiency. Well away from resonances, the scattering cross sections of the glass constituents (Si, O, Li, and a little Ce activator) are slowly varying and the only effect included beyond exponential transmission and average capture probability after scattering is the average energy loss (90° elastic scattering) before capture. Resonances considered significant with approximate parameters are shown in the accompanying Table IV.

TABLE IV. Resonances contributing to enchancement of sensitivity and to transmission loss in a 0.05-cm ^{6}Li glass scintillator flux monitor (see Fig. 1).

Isotope	E_n^0 (keV)	σ_0 (b)	$\Gamma/2$ (keV)
^{140}Ce	1.30	~2000	0.020
^{28}Si	55.5	47	0.36 [a]
^{28}Si	187	15	20 [b]
^{6}Li, ^{7}Li	250	10.1	~45
^{16}O	442	11.8	23
^{28}Si	570	8.4	12
^{16}O	1000	5.2	50
^{16}O	1312	4.0	21
^{16}O	1651	6.3	2 [a]

[a] Instrumental broadening significant.
[b] Resonance-potential interference was included.

Those which are very narrow are marked with an a, indicating that experimental resolution broadening should be included. This was done by root-mean-square addition of moderation time and neutron burst duration contributions for a particular flight-path length.

The broad ^{28}Si resonance at 187 keV shows substantial resonance-potential interference which should be included. The asymmetric lithium resonance-scattering cross section near 250 keV was conveniently approximated as a linearly increasing fraction of the ^{6}Li$(n,\alpha T)$ cross section from 140 to 240 keV and a constant 60% thereof from 240 to 880 keV. The ^{6}Li$(n,\alpha T)$ cross section, of course, was computed carefully from Uttley's parameters, to which a term $0.20/\{1.+[E\text{-}2000./860.)^2/E]\}$ b was added to better reproduce the cross section from 550 to 2000 keV. The rapid energy change of the ^{6}Li$(n,\alpha T)$ cross section over the 250-keV resonance and the large energy loss on scattering from ^{6}Li necessitated a second call to the cross-section routine for the scattered components in this region whereas at lower energies the $(n,\alpha T)$ cross section could be taken as proportional to $E^{-1/2}$ or flat over narrow intervals.

APPENDIX II.

The total γ-ray energy weighting technique also permits the ready calculation of an average γ energy. As the excitation energy is dependent on the incident neutron energy as well as the binding energy, it is convenient to form the ratio

$$\nu = E_x / \overline{E}_\gamma \ .$$

This quantity is closely analagous to the average multiplicity traditionally measured by coincidence techniques and may, in favorable cases, correlate with compound-state spin values.[23]

The average total γ-energy weighting function calculated from the data gives the energy per γ ray actually detected and must be corrected for the detector efficiency and solid angle. These quantities are computed from the geometry and composition of the scintillator cells and the photon cross sections (primarily the Compton cross section) in the computer code that generates the weighting function. The average efficiency for a particular nuclide and resonance is approximated by the efficiency for a single γ ray having the average energy found. For compound states decaying only to the ground state this is trivially exact. At the opposite extreme with high level densities and no high-energy γ-ray enhancement, the distribution of γ energies approximates a Maxwellian with $kT \approx 1.0$ MeV, cutoff at the binding energy, and the multiplicity may be high

[$\nu = 3.8$ for $BE = 5.7$ MeV for (^{164}Dy + n)]. The correlation factor was parametrized to ± 2% as

$$E_\gamma = 0.204\,\overline{G}^{0.715}$$

over the energy range 0.85–10 MeV and the effect of using the efficiency at $\overline{E}_\gamma$ to approximate the efficiency averaged over the extreme case of the Maxwellian distribution was evaluated. The average energy was estimated to ± 3% standard deviation.

---

*Research sponsored by the U. S. Atomic Energy Commission under contract with the Union Carbide Corporation.

†Present address: Australian Atomic Energy Commission, Lucas Heights, Australia.

‡Present address: Denison University, Granville, Ohio.

[1]J. A. Farrell, G. C. Kyker, Jr., E. G. Bilpuch, and H. W. Newson, Phys. Lett. 17, 286 (1965).

[2]E. M. Burbidge, C. R. Burbidge, W. A. Fowler, and F. Hoyle, Rev. Mod. Phys. 29, 547 (1957).

[3]D. D. Clayton, Astrophys. J. 139, 637 (1964).

[4]RENDA, EANDC 85 U, 1970 (unpublished) and NCSAC, WASH-1144, 1969 (unpublished).

[5]N. C. Pering and T. A. Lewis, IEEE Trans. Nucl. Sci. NS16, 3, 316 (1969).

[6]R. L. Macklin, Nucl. Instrum. Methods 91, 79 (1971).

[7]R. L. Macklin and B. J. Allen, Nucl. Instrum. Methods 91, 565 (1971).

[8]R. L. Macklin and J. H. Gibbons, Phys. Rev. 159, 1007 (1967).

[9]N. A. Betz, J. W. Reynolds, and G. G. Slaughter, USAEC Division of Technical Information Report No. CONF 690301, 1969 (unpublished).

[10]Nuclear Enterprises Inc., San Carlos, California.

[11]R. L. Macklin, N. W. Hill, and B. J. Allen, Nucl. Instrum. Methods 96, 509 (1971).

[12]R. Nutt, Rev. Sci. Instr. 39, 1342 (1968).

[13]C. A. Uttley *et al.*, USAEC Report No. CONF 710301 and references therein.

[14]B. J. Allen and R. L. Macklin, Phys. Rev. C 3, 1737 (1971).

[15]J. G. Sullivan, G. G. Warner, R. C. Block, and R. W. Hockenbury, Rensselaer Polytechnic Institute, Troy, New York, USAEC Report No. RPI-328-155, 1969 (unpublished).

[16]J. L. Fowler and E. C. Campbell, Phys. Rev. 127, 2192 (1962).

[17]J. L. Fowler, Phys. Rev. 147, 870 (1966).

[18]C. D. Bowman *et al.*, Phys. Rev. Lett. 25, 1302 (1970).

[19]B. J. Allen and R. L. Macklin, USAEC Report No. CONF-710301, 1971 (unpublished), Vol. 2, p. 764.

[20]B. J. Allen, R. L. Macklin, C. Y. Fu, and R. R. Winters, Phys. Rev. C 7, 2598–2600 (1973).

[21]C. Y. Fu and F. G. Perey, ORNL Report No. ORNL-4765, 1972 (unpublished).

[22]*Neutron Cross Sections*, compiled by M. D. Goldberg, F. Mughubghub, S. N. Purohit, B. A. Magurno, and V. M. May, Brookhaven National Laboratory Report No. BNL-325 (U. S. GPO, Washington, D. C., 1966), 2nd ed., 2nd Suppl., Vol. IIc, $Z = 61$ to 87.

[23]C. Coceva, F. Corvi, P. Giacobbe, and G. Carraro, in *Proceedings of the Second Conference on Neutron Cross Sections and Technology, Washington, D. C., 4–7 March 1968*, National Bureau of Standards Special Publication No. 299 edited by D. T. Goldman (U. S. GPO, Washington, D. C., 1968), Vol. II, pp. 897–902.